International Journal of Scientific Research in Science, Engineering and Technology
Print ISSN: 2395-1990 | Online ISSN : 2394-4099 (www.ijsrset.com)
doi : https://doi.org/10.32628/IJSRSET

Characterization of AA6063 using activated TIG welding with TiO2 flux

Rajiv Kumar[a], Harmesh Kumar Kansal[b] and S.C. Vettivel [c]
[a]Research Scholar, UIET, Panjab university, Chandigarh, India
[b]Professor, UIET, Panjab University, Chandigarh, India
[c]CCET (Degree Wing), Chandigarh, India

Article Info
Publication Issue :
Volume 10, Issue 1
January-February-2023
Page Number : 55-65
Article History
Accepted : 05 Jan 2023
Published: 19 Jan 2023

ABSTRACT

This paper is focused on the ATIG characterization of Aluminium Alloy (AA) 6063 T6 using TiO2 with the filler of AA 5356. The characterization of the Base Material (BM), Fusion Zone (FZ), Heat Effected Zone (HAZ) and partially melted zone are done using the Optical Microscope, Field Emission Scanning Electron Microscope (FESEM), Energy Dispersive Spectrum (EDS) and electron back scatter diffraction.

Keywords : Aluminum Alloy, Activated TIG welding, Texture, Microstructure

I. INTRODUCTION

A-TIG welding is a technique that can produce an enhanced weld characteristics. There are certain cases because of which the use of this technique is restricted such as inferior weld surface quality and inferior metallurgical and mechanical properties and also its use, especially in industries. Different results are obtained by performing A-TIG welding on different types of steels, Aluminium and fluxes provided [1-2]. Aluminium Alloy (AA) 6063 has god strength and applications [3-4].

In Tungsten Inert Gas (TIG) welding, the arc is generated between tungsten electrode and the work piece [5]. The tungsten electrode and the weld pool are shielded by inert gases [6]. Numbers of efforts have been taken to increase the efficiency and productivity of TIG welding [7]. TIG welding with activating materials is called as Activated TIG (ATIG) which has been favorably used to increase productivity of the process. ATIG welding is used efficiently for producing the joints of high quality with filler rod due to an increase content of globular grains and decreased grain size[8-9].

In ATIG welding, a stripe of flux is layered on the area to be welded after making a mixture with appropriate solvent and TIG welding is done with fillers. Normally used fluxes are normally oxides, chlorides and fluorides. ATIG welding has lead to impressive improvement in the DOP as compared to the conventional TIG[10].

Hemant Kumar and N K Singha [11] used ceramic fluxes to find welding characteristics of 304 austenitic stainless steel welded joints. It was confirmed that there was a positive improvement in DOP.Ravi Shanker Vidyarthy and Dheerendra Kumar Dwivedi

[8,9,12] investigated the ATIG weldments. It is confirmed that the hardness and tensile strength were high as compared to base metal (P91 steel). But the toughness in the ATIG weld zone was lower than the base metal.

Li Hui et al [13] introduced a new welding methods for AA 2219 alloy. The area to be welded was coated with an agent in advance to avoid oxide film and porosity. The direct current electrode negative TIG welding with the help of active agents (AlF, LiF, KF-AlF3 & K2SiF6) had eliminated the welding porosity of AA 2219. Application of the fluxes results in increasing the arc voltage as compared with conventional TIG welding. It improves the DOP and the ratio of depth to width (D/W) of the weldment [13,14]. The increase in DOP enhances the heat flow rate in lateral direction from the weld pool to the BM. The increased heat flow rate from the weld pool causes grain refinement owing to high cooling rate and low solidification time [15]. High (D/W) imparted to the weld pool by activated fluxes is found similar to the high energy density process [16-19]. Even though researchers have studied the effect of fluxes on mechanical behaviour on ATIG welded joints. But nobody has studied the effect on grain size and texture in ATIG welded AA joints using Electron Backscatter Diffraction (EBSD). The mechanical behavior, microstructure and texture characterization of AA 6063 T6 using ATIG with three flux TiO2 are studied. Trials test are conducted to select welding parameters as explained in [20,21,22].

II. Materials and Methods

2.1 Materials

1000*300*6 mm plate of AA6063 T6 was used as BM in this study. The composition and mechanical properties of the AA6063-T6 is listed in Table 1. and for the filler wire is presented in the Table 2. The AA6063-T6 and filler AA 5356 are purchased from Mallinath Metal, Mumbai, Maharashtra, India.

Table 1 AA 6063 T6Chemical Composition

Alloy Weight%	Al	Si	Cu	Mn	Mg	Cr	Fe	Zn
6063-T6	97.9	0.2-0.6	0.1	0.1	0.7	0.1	0.35	0.1

Table 2 Filler Rod AA 5356 Chemical Composition

Alloy Weight%	Al	Si	Fe	Cu	Ti	Zn	Mn	Mg
AA 5356	Bal	0.25	0.40	0.10	0.20	0.10	0.10	4.5

2.1.2 Flux

For this study TiO_2 is chosen. The amount of flux used per job is $3 * 10^{-2}$ mg/mm^2.The flux are bought from Akshar Exim Company Private Limited, Kolkata, West Bengal, India.The compositions of the TiO_2 is given in Table 3.

Table 3 Chemical composition of ceramic fluxes

Molecular Formula	Density g/cm³	Melting Point, °C	Boiling Point, °C	Molecular Weight, g/mol
TiO_2	4.23	1855°C	2973	79.865

2.2. Methods

2.2.1 Preparation of activation mixture

The preparation of activation mixture flux paste is one of the important job in ATIG welding. The mass of the flux required for a welding is calculated from the volume calculation as explained in [1, 7, 9].

2.2.2. ATIG Welding

TIG welding power source (Make: Panasonic, Model BR1-200 (AC/DC), capacity: 250 A with machine torch) with standard argon gas with regulator was used for welding. A 6 mm thick plate was cut into 160 × 75 mm. The surface of the samples were cleaned with acetone. The arc was set to 3-3.5 mm between the electrode tip and work piece. The welding was carried out at 120 mm/min. A 3mm diameter thoriated tungsten electrode was selected in welding. The significant welding variables are as shown Table 4.

Table 4 Welding Parameters

Welding Current, Amps	Welding speed, mm/min	Arc length, Mm	Shielding gas, l/min	Electrode dia. mm
165– 220	120	3-3.5	Pure argon (99.99%) with 9-10 l/min	3

2.3 Non destructive evaluation

Ultrasonic Non-Destructive Evaluation (NDE) is done as per ASTM E164 - 19 standards using A-scan, MODSONIC, digital ultrasonic flaw detector in Modern Engineers & NDE System, Yamunanagar, Haryana, India.

2.4 Characterization

The samples were prepared with the help different grit size varied from 50 to 3000. Alumina paste along with the velvet cloth is used to smooth the surface of the specimen at Chandigarh College of Engineering Technology (Degree Wing), Chandigarh, India. The samples were etched with Keller's reagent after polishing for the Optical Microscope (RADICAL, model RXM 7).The weldment & fractured surface of specimens were analysed using Field Emission Scanning Electron Microscopy (FESEM) (Model: JEOL JSM 7600F) and Energy Dispersive Spectroscopy (EDS) at the Indian Institute of Science Education and Research Mohali, Panjab, India.After electro polishing was done with the help of: 80:20 methanol: Per Chloric acid, 13 V dc and-20^0 C. The grain size and micro texture of the samples were characterised with the help EBSD on FEI Quanta™ Nova Nano SEM.

III. Results and Discussion

3.1 Characterization

3.1.1 OM Characterization

Fig. 1 shows the optical OM images at 400x of the BM, FZ and interface for conventional TIG and ATIG welded joints using flux TiO_2. Three different zones were identified as FZ, partially-melted zone (PMZ), and HAZ. Fig 1(b, d) shows the OM of the images of FZ the conventional TIG and ATIG welded joints. The interfacial microstructure at PMZ of ATIG weldment of AA6063-T6 is shown in Fig. 1(c).In Fig. 1(b &d), dendrites and column dendrites were observed because of the phenomenon of the rapid temperature changes from high to low in FZ at the time of the welding. Fig. 1(b, d) confirm the microstructure in ATIG with flux TiO_2 is finer as compared to the conventional TIG welded joints.

The epitaxial grain form is observed near the fusion boundary. The FZ had columnar dendrites and secondary phases were present as segregates at the inter-dendrite.as shown in Fig. 1(b, d,).The FZ boundary showed random disorientation between BM grains and weldment grains as shown in Fig. 1(c) [22-25]. The PMZ is located near the fusion line. Fig. 1(c) confirms that the microstructure varies largely towards the centre of weld from the edge of fusion line The size of grains in HAZ of conventional TIG is more as compared to ATIG with flux TiO_2 [26].

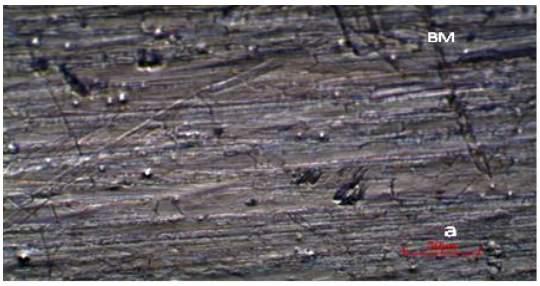

(a)

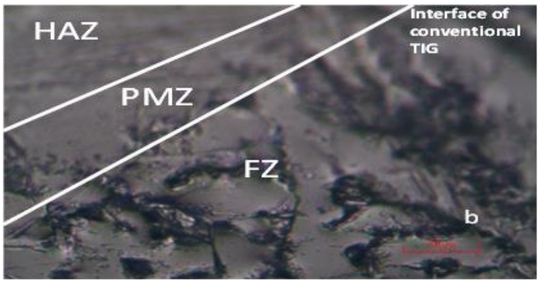

(b)

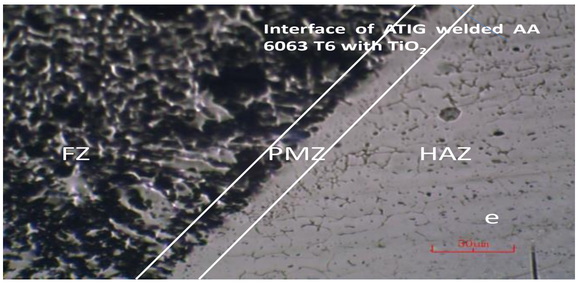

(c)

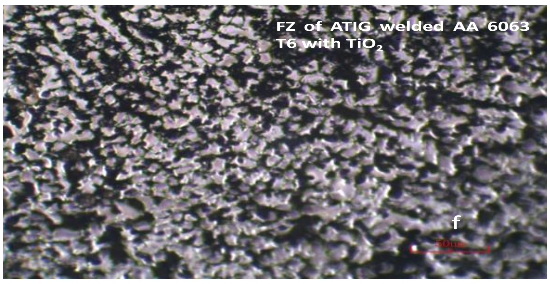

(d)

Fig. 1 OM images of AA 6063-T6 with conventional TIG and ATIG (a) BM (b) FZ of conventional TIG (c) interface of ATIG using TiO_2 (d) FZ of ATIG using TiO_2

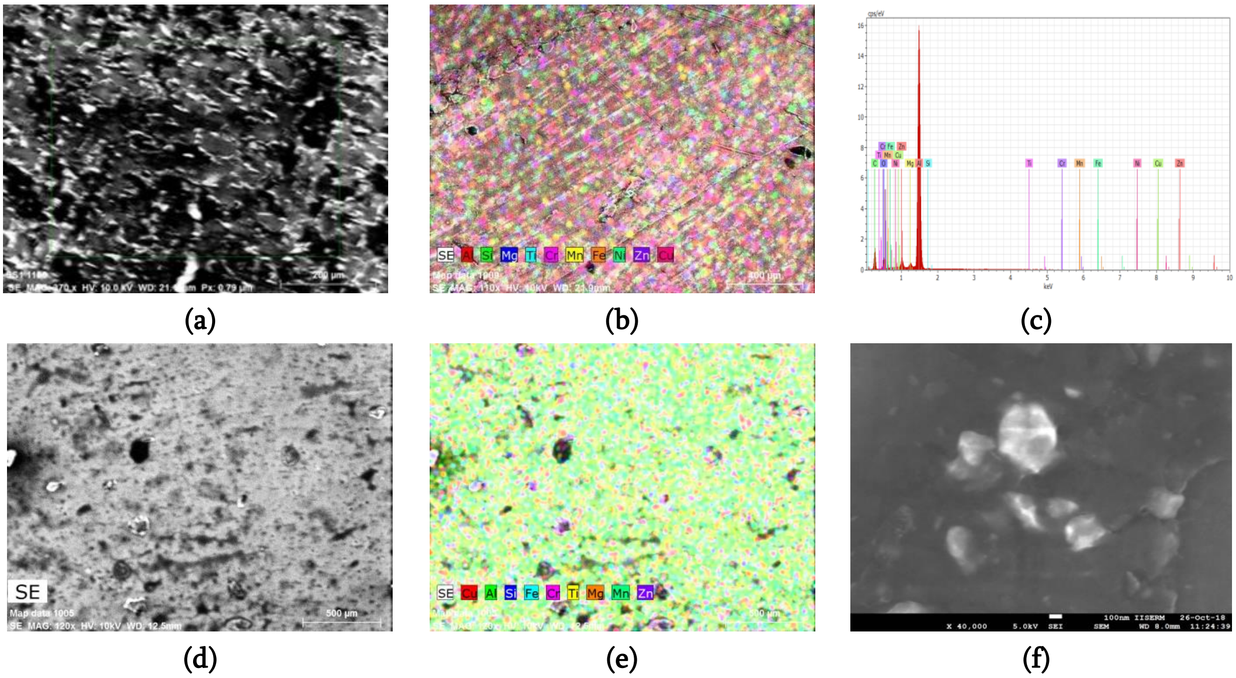

Fig. 2(a-c) SEM & EDS of BM (d-f) SEM- EDS of ATIG using TiO_2

SEM- EDS Analysis : SEM-EDS mapping are used to characterize the BM and weldments as well as to determine elemental composition of the BM, conventional TIG and ATIG with fluxes TiO2 as shown in Fig. 2. The SEM & EDS analysis of BM AA 6063-T6 is presented in Fig. 2(a - c).The element identified are Si, Zn Mg, Cu, Ni, Ti, Fe and Cr. The main element observed in AA 6063-T6 are Mg and Si. It is also seen that there was no drastic change in composition of the FZ of ATIG welding with flux TiO_2 . A typical i precipitates of Fe, Mg, and Si are identified.The EDS map analysis, represents that nuclei are rich in Si, Ti and Mg. Fig. 2(f) confirmed the precipitates of Mg and Si elements and consisted of Si, Mg_2Si and α-Al8Fe2Si phases as explained in [27–29]

3.2.4 EBSD Analysis

A systematic comparison of the EBSD Inverse Pole Figures (IPFs) is required to quantitatively relate the distribution of microstructure with welding parameters. The shape and size of grain from FZ boundary into FZ centre vary from coarse columnar to and equiaxed in the direction of heat flow. The columnar grains grow normally to the FZ line. It has good agreement with [26].

The texture of the conventional TIG and ATIG were analyzed using Pole Figures (PF). The microstructure of the samples is analyzed and the outcomes are given in Fig. 3 to Fig. 5. A texture ({001} ⟨100⟩) is seen in welded samples. This is mainly due to the epitaxial growth of dendrites columnar shape along ⟨100⟩ direction. It has good agreement with [30].

EBSD grain boundary, PF, IPF and Orientation Density Function (ODF) maps of conventional TIG & ATIG with,TiO_2 at BM, FZ & HAZ are given in Fig. 3 to Fig. 5. The fine and equiaxial grains were found in FZ and recrystallization appears in HAZ and PMZ. In EBSD grain boundary, PF & IPF the blue represents <111> ,green <110>and red<001>. The Fig. 3(a), Fig. 45(a) and Fig. 5(a) shows the EBSD grain boundary, PF and IPF maps of BM. They confirm that material grains are oriented near to <111>and partly to <001> and in HAZ of ATIG welding with TiO_2 the orientation is <001> and partially <111>.It has good agreement with [31].

In FZ texture changes and intensity decreases in ATIG welding with flux TiO_2 & as compared to BM due to the pinning of grain boundaries in FZ and HAZ. Also due to high temperature thermal cycles which deplete texture. Columnar grains grow normal to FZ line as shown in Fig 5.This is due to recrystallisation. [32].

In Fig. 3, the FZ of ATIG welding with TiO_2 exhibits equiaxed grains and Low Angle Grain Boundaries (LAGB) as compared to conventional TIG. The Fig. 4(a-d) reveals that the mean grain size in FZ of ATIG welding with fluxes TiO_2 and conventional TIG varies from 50, to 90 μm respectively. The Kernel Average Misorientation (KAM) bar charts are presented in Fig 4(a-d). KAM bar charts reveal that the average disorientation of every neighboring pixel with one another. The mean disorientation in an area shows the energy stored. The red and blue indicates the high and low deformed area respectively. The low values of KAM plots in FZ confirm the recrystallisation. It is in good agreement with [31].

It is also confirmed that TiO_2 enhanced the grain refinement [26, 34]. It is also confirmed that grain size in FZ of conventional TIG is more than FZ of ATIG welding with TiO_2. The average grain size in FZ is less than HAZ .This is mainly due to the dissolution of the precipitates resulted at the time of local heating and re-precipitation at the time of cooling.

The PF {100}[110],{111}[113] for ATIG with fluxTiO_2, BM and conventional TIG is given in Fig.5 It indicated the texture of FZ is symmetric due to uniform nucleation and plastic deformation. In Fig. 5(a&c) the FZ region contain {001}<100>,{011}<100>orientation. After the rotation through 9 degree around A1 and 14 degrees through A2 the same component was observed and the region take the component containing {001}<110>,{011}<112>,{110}<223>,{001}<110> and {223}<112> orientation. It is in good agreement with [24, 25].

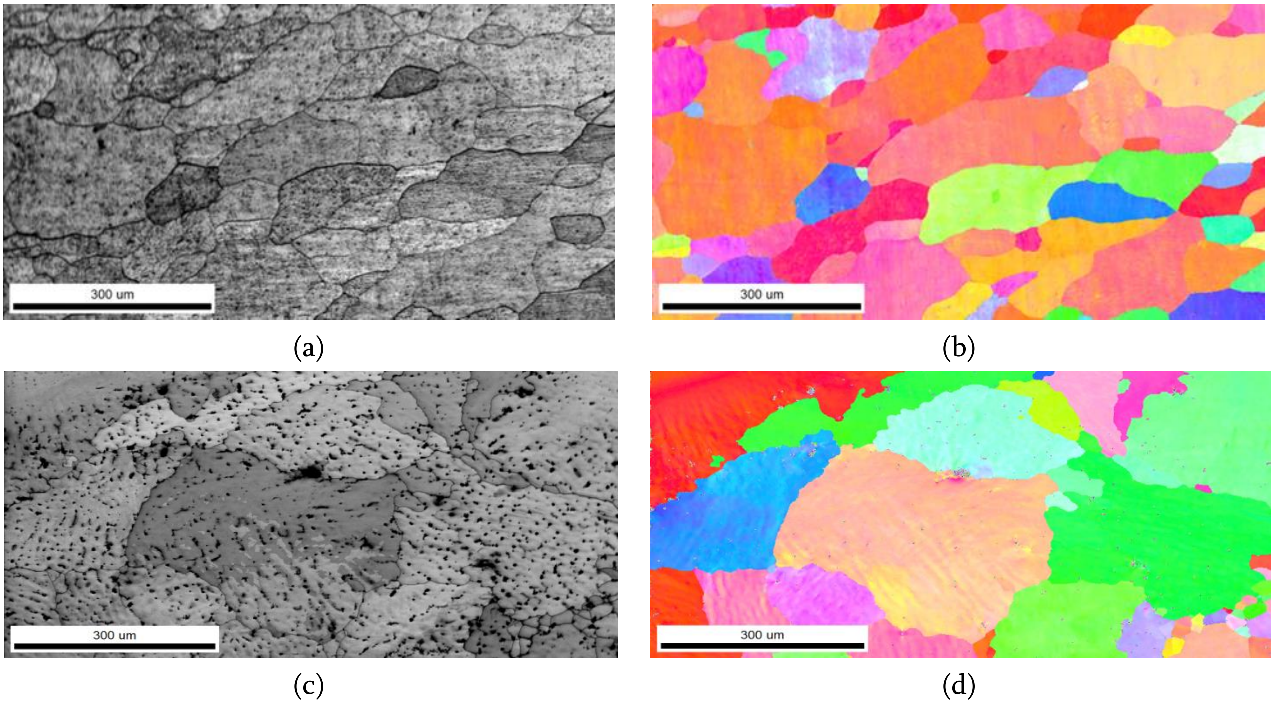

Fig. 3 SEM and EBSD grain-boundary of BM and ATIG of AA 6063-T6 using flux TiO_2 (a) SEM of BM (b) EBSD of BM (c) SEM of ATIG using TiO_2 (d) EBSD of ATIG using TiO_2

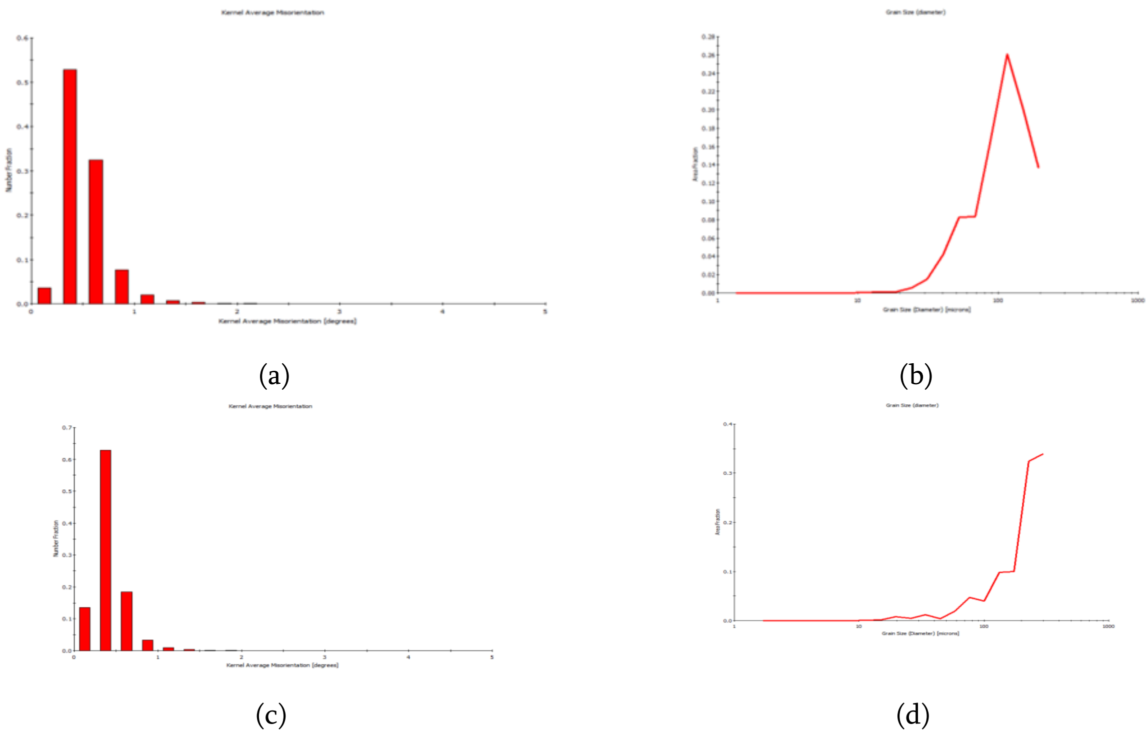

Fig. 4 Distribution of KAM and grain Size of BM AA 6063-T6 and ATIG welded with fluxes (TiO_2 & Al_2O_3) (a) KAM of BM (b)grain Size of BM ((c) KAM of ATIG using TiO_2 (d) grain Size of ATIG using

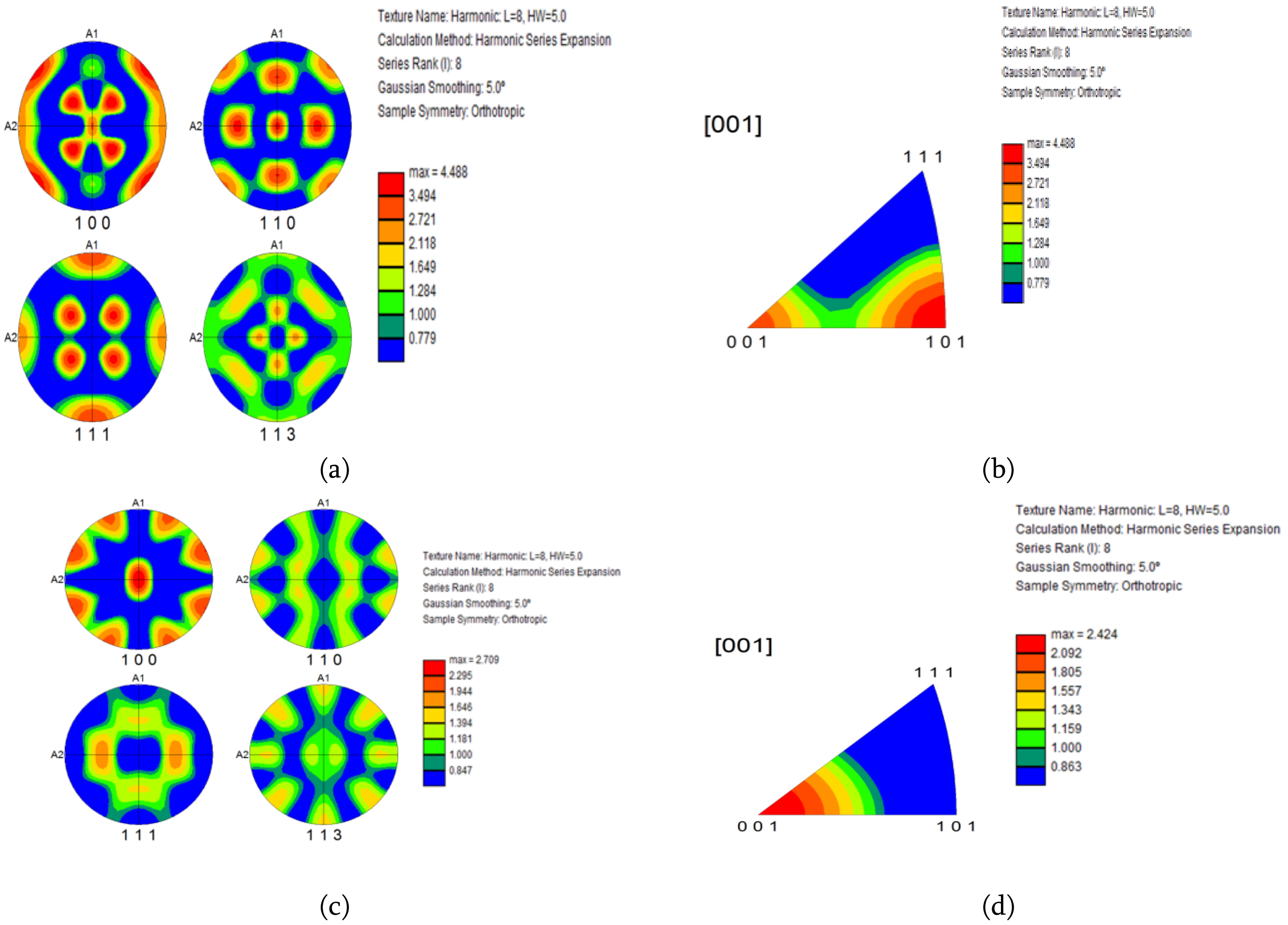

Fig. 5 PF and IPF for conventional TIG and ATIG with flux TiO_2 (a) PF of conventional TIG (b) IPF of conventional TIG (e) PF of ATIG using TiO_2 (f)IPF of ATIG using TiO_2

IV. CONCLUSION

ATIG welding with ceramic fluxes (SiO_2, TiO_2 and Al_2O_3) and conventional TIG welding of AA6063 T6 with filler AA 5356 were carried out at different current and gas flow rate. The influence of ceramic flux TiO_2 on the microstructure & texture were studied and the following conclusions are drawn:

- Fine equiaxed grains exist in FZ and coarsened equiaxed grains are visible HAZ. The width of HAZ increases with increase of the heat input. Grain size measurements confirmed that the HAZ contains coarse grains than the BM.
- FESEM and EDS confirmed the presence of Fe, Mg and Si which resulted in the formation of Al-Fe-Si intermetallic phases during solidification. Silicon combines with magnesium to form Mg_2Si phase during the solidification. The region of the weld revealed a fully recrystallized fine grain structure.
- PF indicates the texture of the FZ is symmetric due to uniform nucleation and plastic deformation.The intensity of texture is reducing from 25 in BM to 11in HAZ and 5 in FZ. This confirmed that the welded samples having weak texture as compared to BM in ATIG welded samples.

V. REFERENCES

[1]. Davis JR, Aluminum and aluminum alloys, ASM Speciality Handbook, ASM International, Materials Park, USA 1994 :1-11

[2]. S.T. Amancio-Filho, S. Sheikhi, J.F. dos Santos, C. Bolfarini, Preliminary study on the microstructure and mechanical properties of dissimilar friction stir welds in aircraft aluminium alloys 2024-T351 and 6056-T4, J. Mater. Process. Technol. 206 (2008) 132–142. doi:10.1016/j.jmatprotec.2007.12.008.

[3]. P. Mukhopadhyay, Alloy Designation, Processing, and Use of AA6XXX Series Aluminium Alloys, ISRN Metall. 2012 (2012) 1–15. doi:10.5402/2012/165082.

[4]. B. Choudhury, M. Chandrasekaran, Investigation on welding characteristics of aerospace materials - A review, Mater. Today Proc. 4 (2017) 7519–7526. doi:10.1016/j.matpr.2017.07.083.

[5]. R.R. Ambriz, V. Mayagoitia, I.P.N. Ciitec-ipn, Welding of Aluminum Alloys, Welding, Brazing Solder. (2018) 722–739. doi:10.31399/asm.hb.v06.a0001436.

[6]. P.J. Modenesi, The chemistry of TIG weld bead formation, Weld. Int. 29 (2015) 771–782. doi:10.1080/09507116.2014.932990.

[7]. A.K. Singh, V. Dey, R.N. Rai, Techniques to improveweld penetration in TIG welding (A review), Mater. Today Proc. 4 (2017) 1252–1259. doi:10.1016/j.matpr.2017.01.145.

[8]. R.S. Vidyarthy, D.K. Dwivedi, Activating flux tungsten inert gas welding for enhanced weld penetration, J. Manuf. Process. 22 (2016) 211–228. doi:10.1016/j.jmapro.2016.03.012.

[9]. R.S. Vidyarthy, D.K. Dwivedi, Microstructural and mechanical properties assessment of the P91 A-TIG weld joints, J. Manuf. Process. 31 (2018) 523–535. doi:10.1016/j.jmapro.2017.12.012.

[10]. K.D. Ramkumar, V. Varma, M. Prasad, N.D. Rajan, N.S. Shanmugam, Effect of activated flux on penetration depth, microstructure and mechanical properties of Ti-6Al-4V TIG welds, J. Mater. Process. Technol. 261 (2018) 233–241. doi:10.1016/j.jmatprotec.2018.06.024.

[11]. H. Kumar, N.K. Singh, Performance of activated TIG welding in 304 austenitic stainless steel welds, Mater. Today Proc. 4 (2017) 9914–9918. doi:10.1016/j.matpr.2017.06.293.

[12]. R.S. Vidyarthy, A. Kulkarni, D.K. Dwivedi, Study of microstructure and mechanical property relationships of A-TIG welded P91–316L dissimilar steel joint, Mater. Sci. Eng. A. 695 (2017) 249–257. doi:10.1016/j.msea.2017.04.038.

[13]. B. Wu, B. Wang, X. Zhao, H. Peng, Effect of active fluxes on thermophysical properties of 309L stainless-steel welds, J. Mater. Process. Technol. 255 (2018) 212–218. doi:10.1016/j.jmatprotec.2017.12.018.

[14]. Y. Huang, D. Fan, Q. Fan, Study of mechanism of activating flux increasing weld penetration of AC A-TIG welding for aluminum alloy, Front. Mech. Eng. China. 2 (2007) 442–447. doi:10.1007/s11465-007-0076-9.

[15]. Q. Li, A. Wu, Y. Li, G. Wang, D. Yan, J. Liu, Influence of temperature cycles on the microstructures and mechanical properties of the partially melted zone in the fusion welded joints of 2219 aluminum alloy, Mater. Sci. Eng. A. 623 (2015) 38–48. doi:10.1016/j.msea.2014.11.047.

[16]. A.K.C. Mills, B.J. Keene, R.F. Brooks, A. Shirali, I. Phenomena, P. Apr, Marangoni Effects in Welding Source : Philosophical Transactions : Mathematical , Physical and Engineering Sciences , Vol . Marangoni effects in welding, 356 (2018) 911–925.

[17]. E.A. Skvortsov, Role of electronegative elements in contraction of the arc discharge, Weld. Int. 12 (1998) 471–475. doi:10.1080/09507119809448517.

[18]. V. Arunkumar, M. Vasudevan, V. Maduraimuthu, V. Muthupandi, Effect of activated flux on the microstructure and mechanical properties of 9Cr-1Mo steel weld

joint, Mater. Manuf. Process. 27 (2012) 1171–1177. doi:10.1080/10426914.2011.610212.

[19]. K.H. Tseng, Development and application of oxide-based flux powder for tungsten inert gas welding of austenitic stainless steels, Powder Technol. 233 (2013) 72–79. doi:10.1016/j.powtec.2012.08.038.

[20]. E.R. Imam Fauzi, M.S. Che Jamil, Z. Samad, P. Muangjunburee, Microstructure analysis and mechanical characteristics of tungsten inert gas and metal inert gas welded AA6082-T6 tubular joint: A comparative study, Trans. Nonferrous Met. Soc. China (English Ed. 27 (2017) 17–24. doi:10.1016/S1003-6326(17)60003-7.

[21]. R.S. Coelho, A. Kostka, J.F. dos Santos, A. Kaysser-Pyzalla, Friction-stir dissimilar welding of aluminium alloy to high strength steels: Mechanical properties and their relation to microstructure, Mater. Sci. Eng. A. 556 (2012) 175–183. doi:10.1016/j.msea.2012.06.076.

[22]. A.S. Zoeram, S.H.M. Anijdan, H.R. Jafarian, T. Bhattacharjee, Welding parameters analysis and microstructural evolution of dissimilar joints in Al/Bronze processed by friction stir welding and their effect on engineering tensile behavior, Mater. Sci. Eng. A. 687 (2017) 288–297. doi:10.1016/j.msea.2017.01.071.

[23]. K.H. Dhandha, V.J. Badheka, Effect of activating fluxes on weld bead morphology of P91 steel bead-on-plate welds by flux assisted tungsten inert gas welding process, J. Manuf. Process. 17 (2015) 48–57. doi:10.1016/j.jmapro.2014.10.004.

[24]. H.T. Fujii, H. Endo, Y.S. Sato, H. Kokawa, Interfacial microstructure evolution and weld formation during ultrasonic welding of Al alloy to Cu, Mater. Charact. 139 (2018) 233–240. doi:10.1016/j.matchar.2018.03.010.

[25]. Q. Chu, R. Bai, H. Jian, Z. Lei, N. Hu, C. Yan, Microstructure, texture and mechanical properties of 6061 aluminum laser beam welded joints, Mater. Charact. 137 (2018) 269–276. doi:10.1016/j.matchar.2018.01.030.

[26]. V.V.M. Krishna G, P.K. Satyanarayana, Microstructure and Mechanical properties of Multipass Friction Stir Processed Aluminum Silicon Carbide Metal Matrix, Int. J. Sci. Eng. Technol. 4 (2015) 88–90. doi:10.17950/ijset/v4s2/212.

[27]. M. Peel, A. Steuwer, M. Preuss, P.J. Withers, Microstructure, mechanical properties and residual stresses as a function of welding speed in aluminium AA5083 friction stir welds, Acta Mater. 51 (2003) 4791–4801. doi:10.1016/S1359-6454(03)00319-7.

[28]. O.R. Myhr, O. Grong, Process Modelling Applied To 6082-T6 a L U M I N I U M Weldments--I . Reaction Kinetics, Acta Metall. Mater. 39 (1991) 2693–2702.

[29]. S. Liu, G. Mi, F. Yan, C. Wang, P. Jiang, Correlation of high power laser welding parameters with real weld geometry and microstructure, Opt. Laser Technol. 94 (2017) 59–67. doi:10.1016/j.optlastec.2017.03.004.

[30]. B. Wang, B.B. Lei, J.X. Zhu, Q. Feng, L. Wang, D. Wu, EBSD study on microstructure and texture of friction stir welded AA5052-O and AA6061-T6 dissimilar joint, Mater. Des. 87 (2015) 593–599. doi:10.1016/j.matdes.2015.08.060.

[31]. K. Zhang, H. Zhou, L. Ni, Y. Chen, A comparative study of microstructure and tensile properties of Ti2AlNb joints prepared by laser welding and laser-additive welding with the addition of filler powder, J. Mater. Process. Technol. 255 (2018) 477–487. doi:10.1016/j.jmatprotec.2017.12.044.

Cite this article as :

Rajiv Kumar, Harmesh Kumar Kansal, S. C. Vettivel, "Characterization of AA6063 using activated TIG welding with TiO2 flux", International Journal of Scientific Research in Science, Engineering and Technology (IJSRSET), Online ISSN : 2394-4099, Print ISSN : 2395-1990, Volume 10 Issue 1, pp. 55-65, January-February 2023.
Journal URL : https://ijsrset.com/IJSRSET231018